INTERNATIONAL ATOMIC ENERGY AGENCY
UNITED NATIONS EDUCATIONAL, SCIENTIFIC AND CULTURAL ORGANIZATION

INTERNATIONAL CENTRE FOR THEORETICAL PHYSICS
34100 TRIESTE (ITALY) - P.O.B. 586 - MIRAMARE - STRADA COSTIERA 11 - TELEPHONES: 224281/2/3/4/5/6
CABLE: CENTRATOM - TELEX 460392 - I

H4.SMR/164 - 15

WORKSHOP ON CLOUD PHYSICS AND CLIMATE

23 November - 20 December 1985

CLOUD AND PRECIPITATION PROCESSES

(A Survey of Observations and Models)

PART 1

GABOR VALI

University of Wyoming

FOGS

LIQUID OR SOLID

DEFINITIONS

IMPACTS

VISIBILITY

$$V = \frac{\ln 0.02}{\sigma} \qquad I = I_0 e^{-\sigma x}$$

$$\sigma = \sigma_{SCAT} = \Sigma \pi r_i^2 N_i k_i$$

$V \propto \frac{\bar{r}}{LWC}$ - CONST. VARIES

$V = a(LWC)^{-b}$ - EMPIRICAL

V =	1-5 km	<1 km	<0.5 km	<0.1 km
	LIGHT		DENSE	V. DENSE

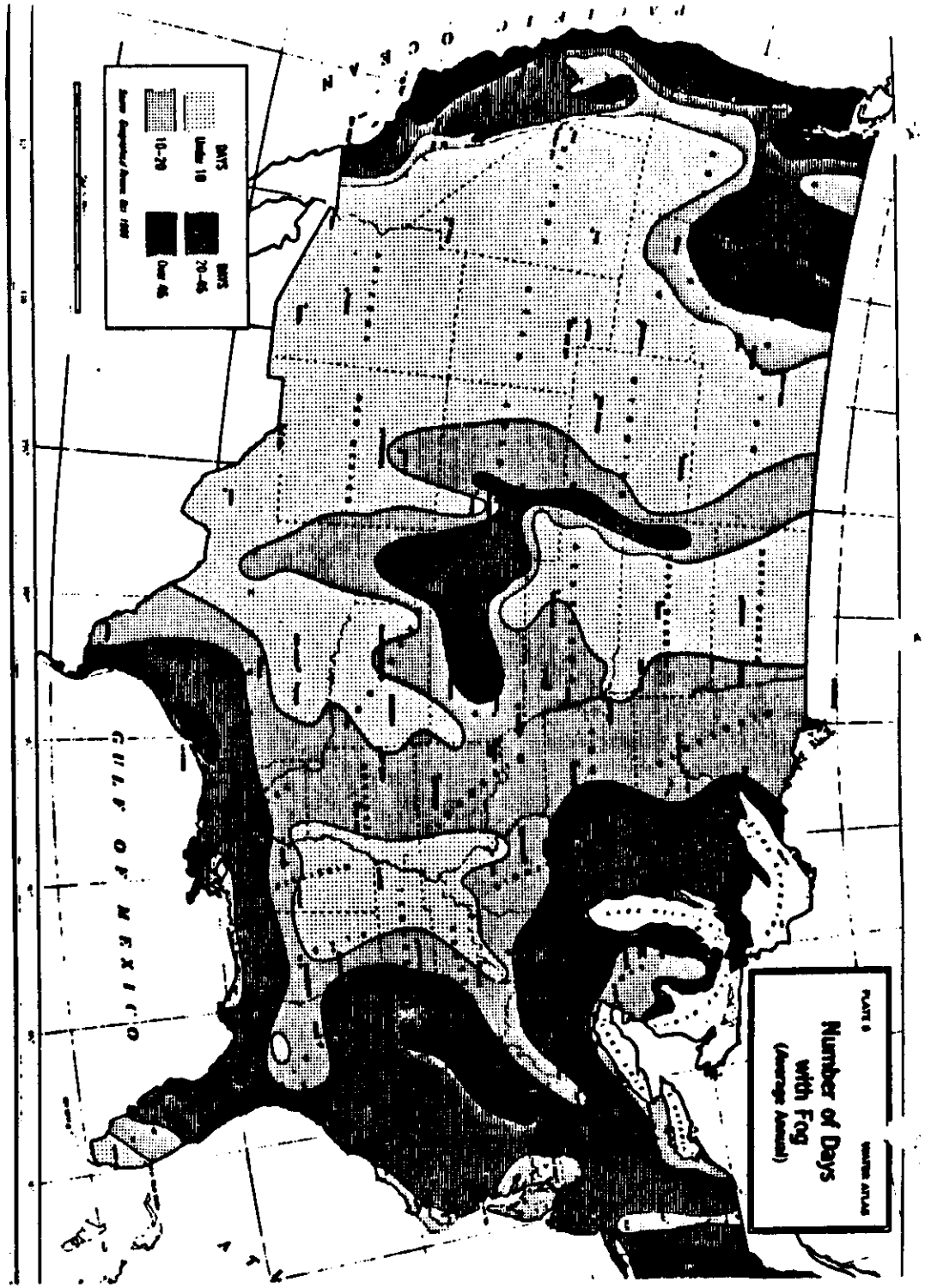

TYPES OF FOG

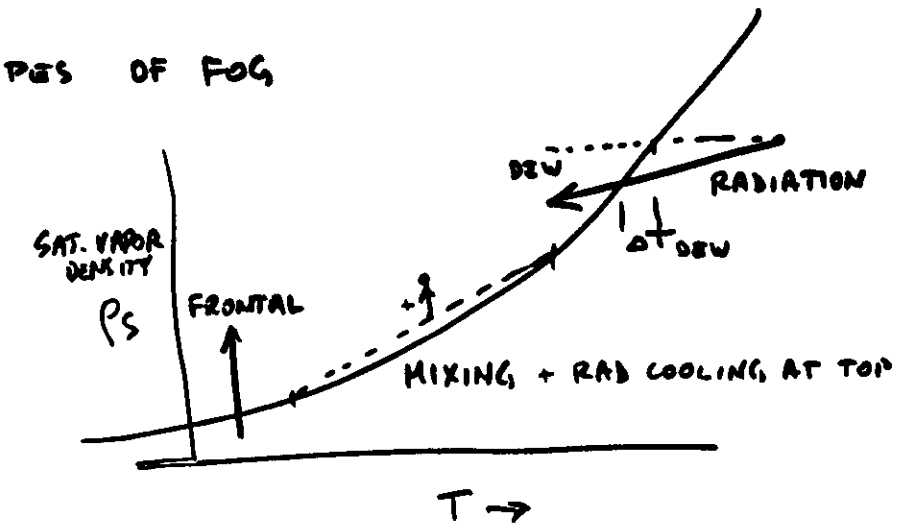

ADVECTION	RADIATION	FRONTAL	OTHER
SEA SPC.	GROUND	PRE-	ICE
LAND, SEA BREEZE	UPSLOPE	POST-	SNOW
	VALLEY		
MIX	COOL	ADD VAPOR	

MICROSTRUCTURE

DYNAMICS
- INVERSION
- VERT. TRANSPORT
- LOCAL CIRCULATIONS

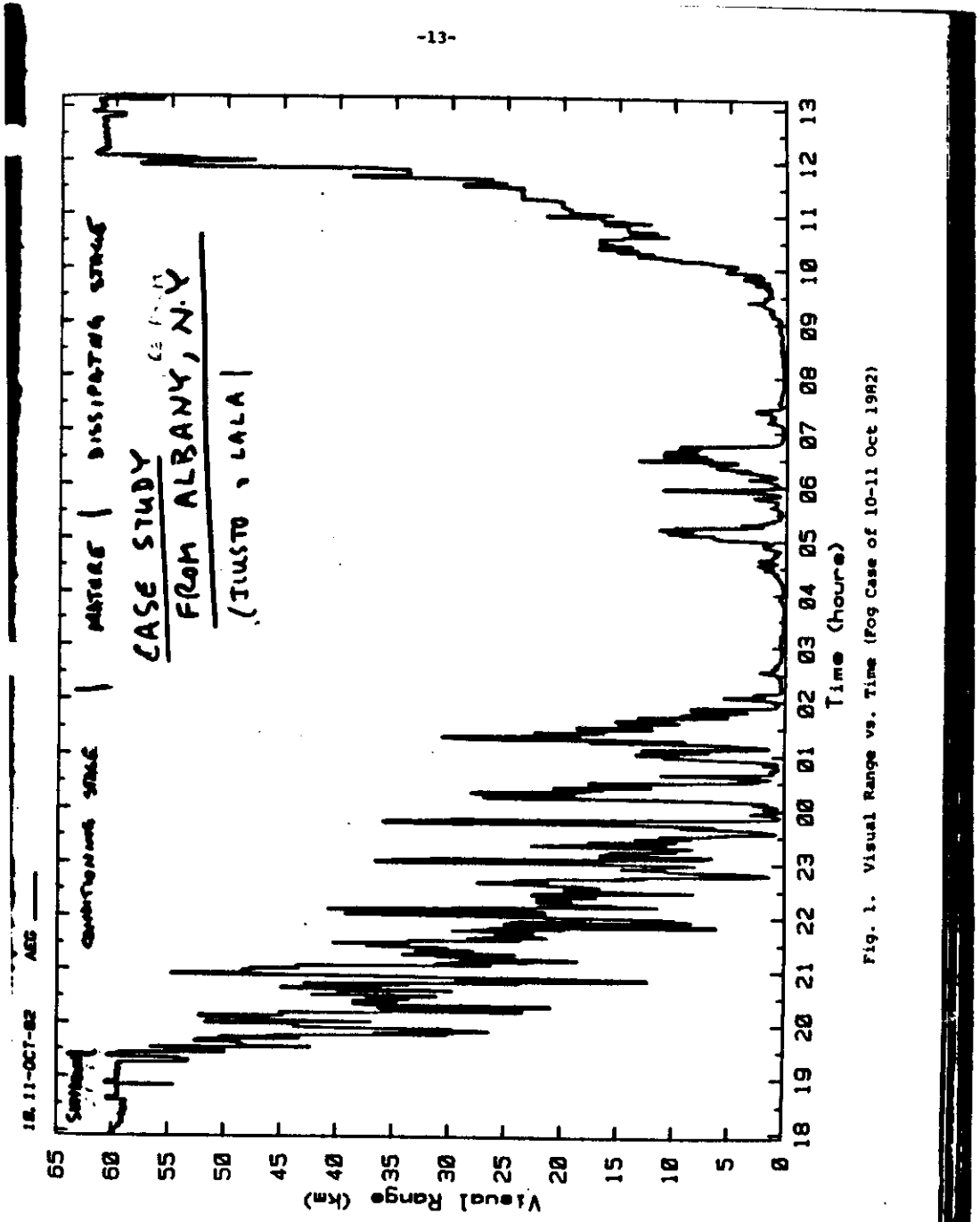

Fig. 1. Visual Range vs. Time (Fog Case of 10-11 Oct 1982)

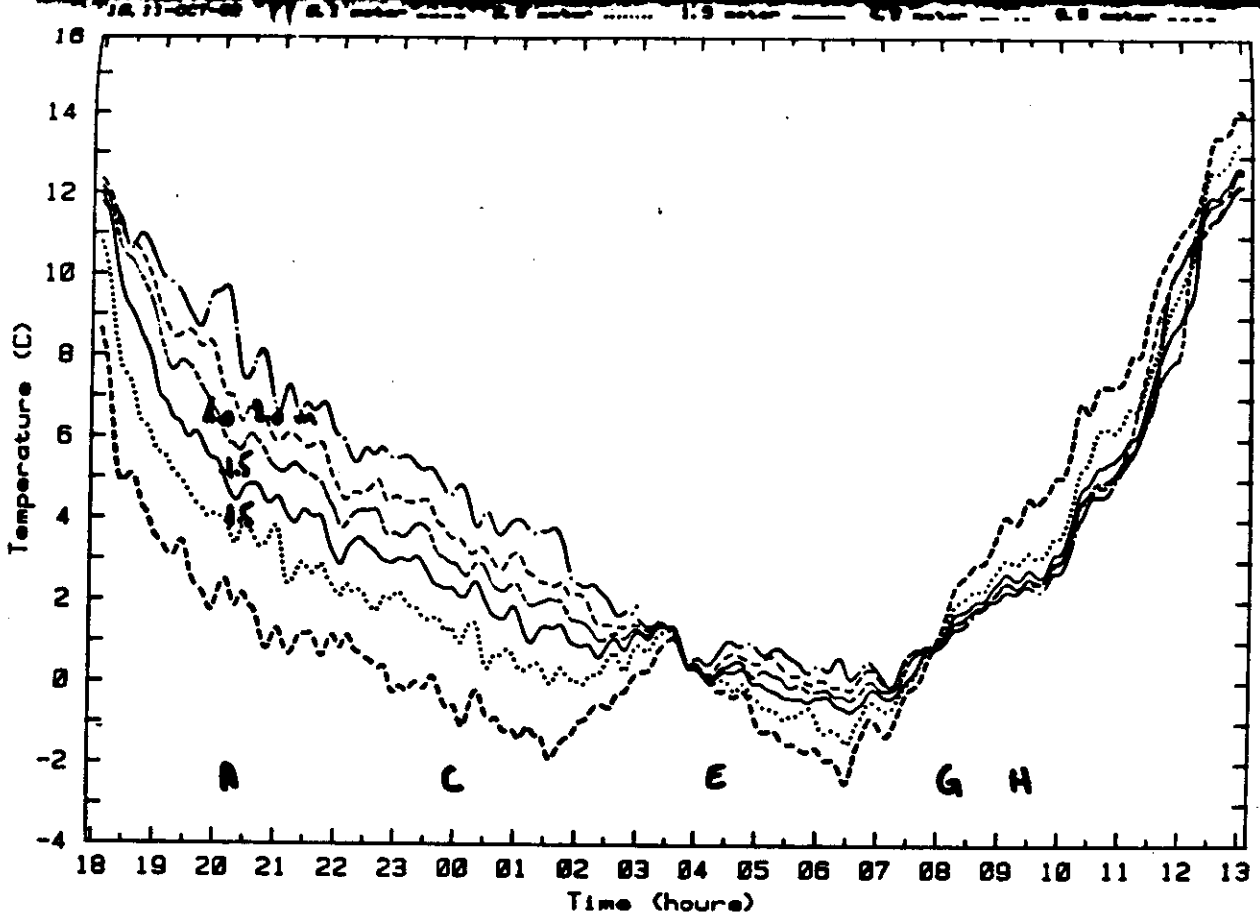

Fig. 2. Temperatures at Selected Levels vs. Time (10-11 Oct 1982)

(3)

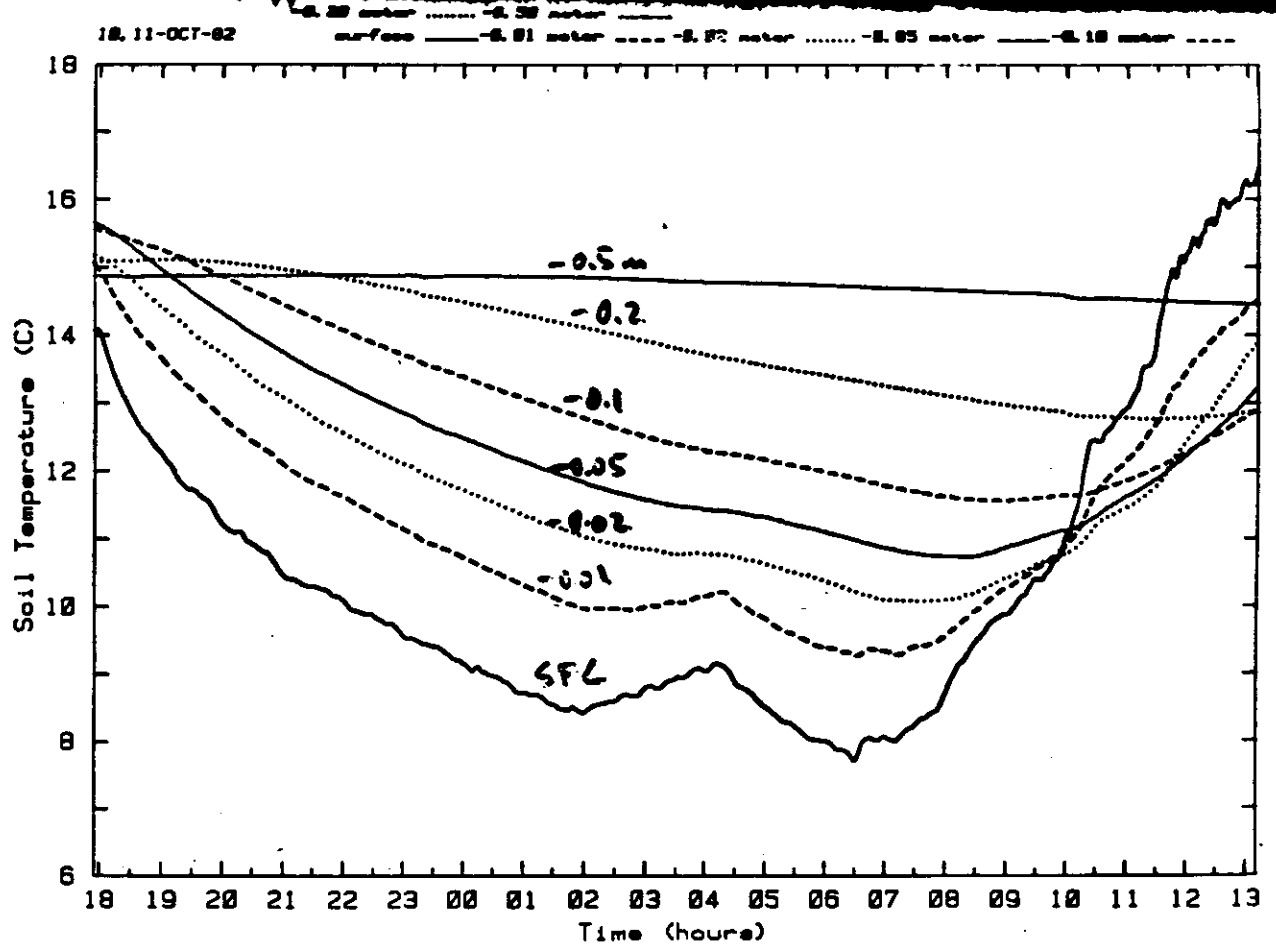

Fig. 8 Soil Temperature vs. Time and Depth

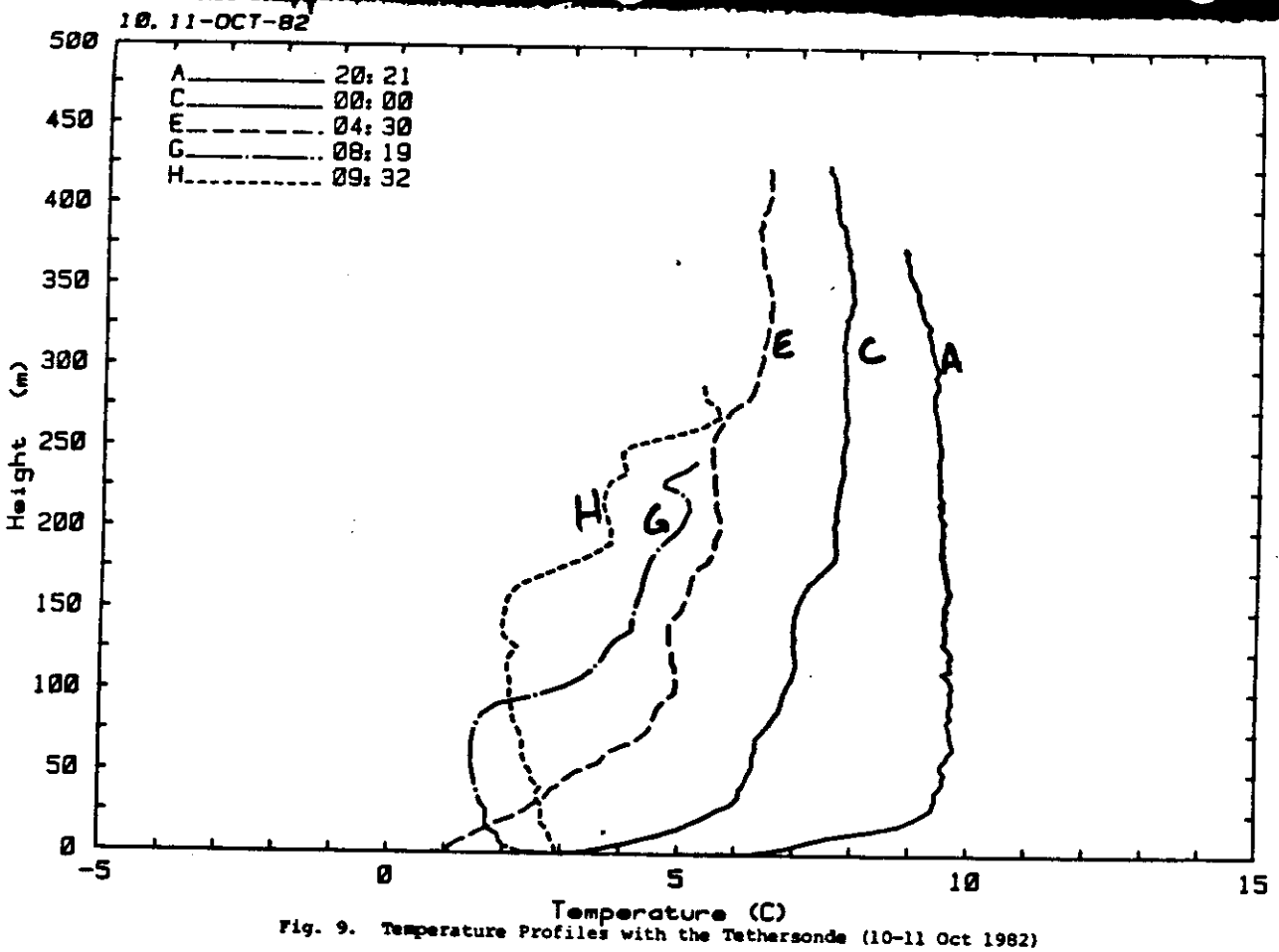

Fig. 9. Temperature Profiles with the Tethersonde (10-11 Oct 1982)

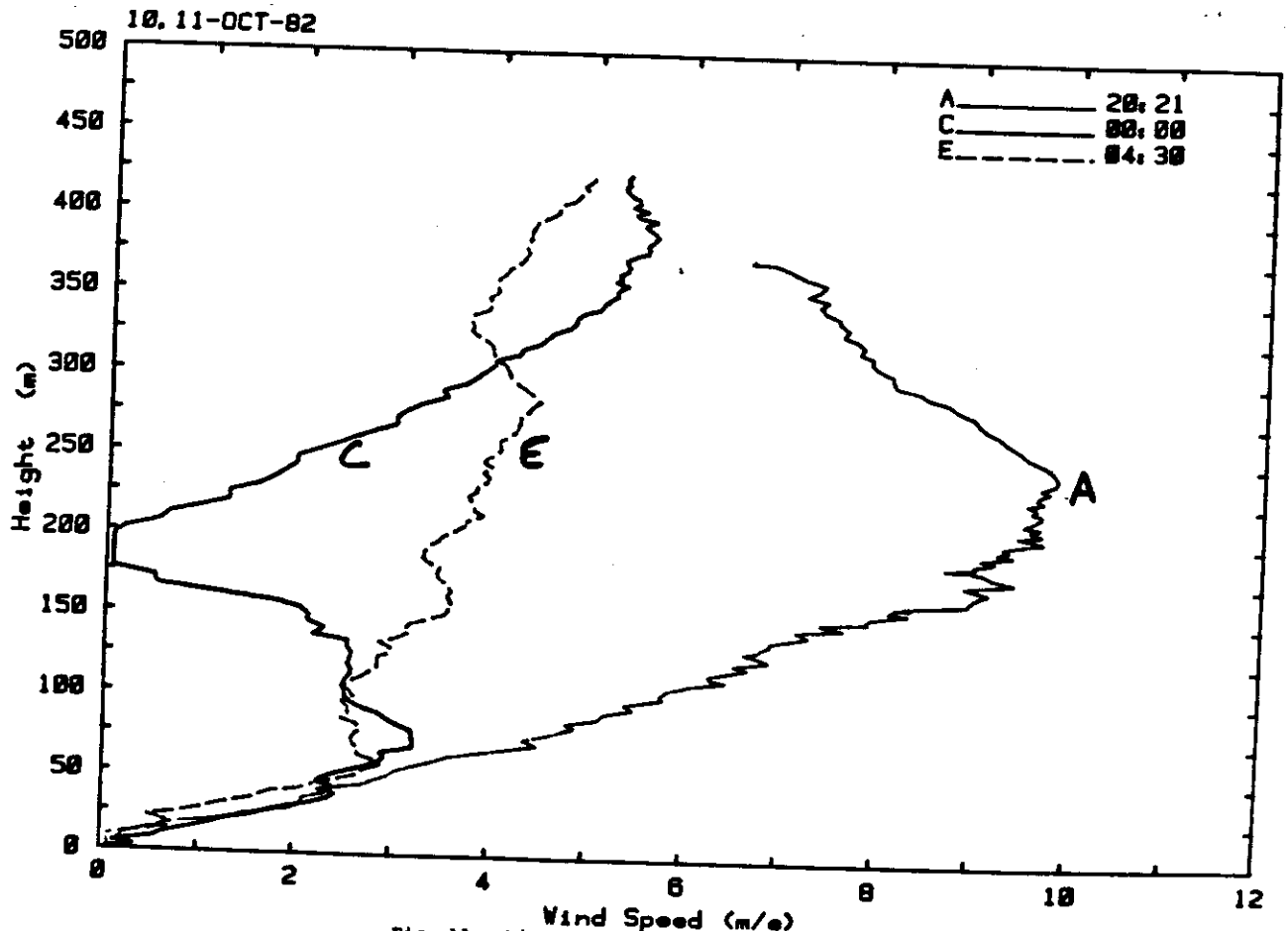

Fig. 11. Wind Speed Profiles (10-11 Oct 1982)

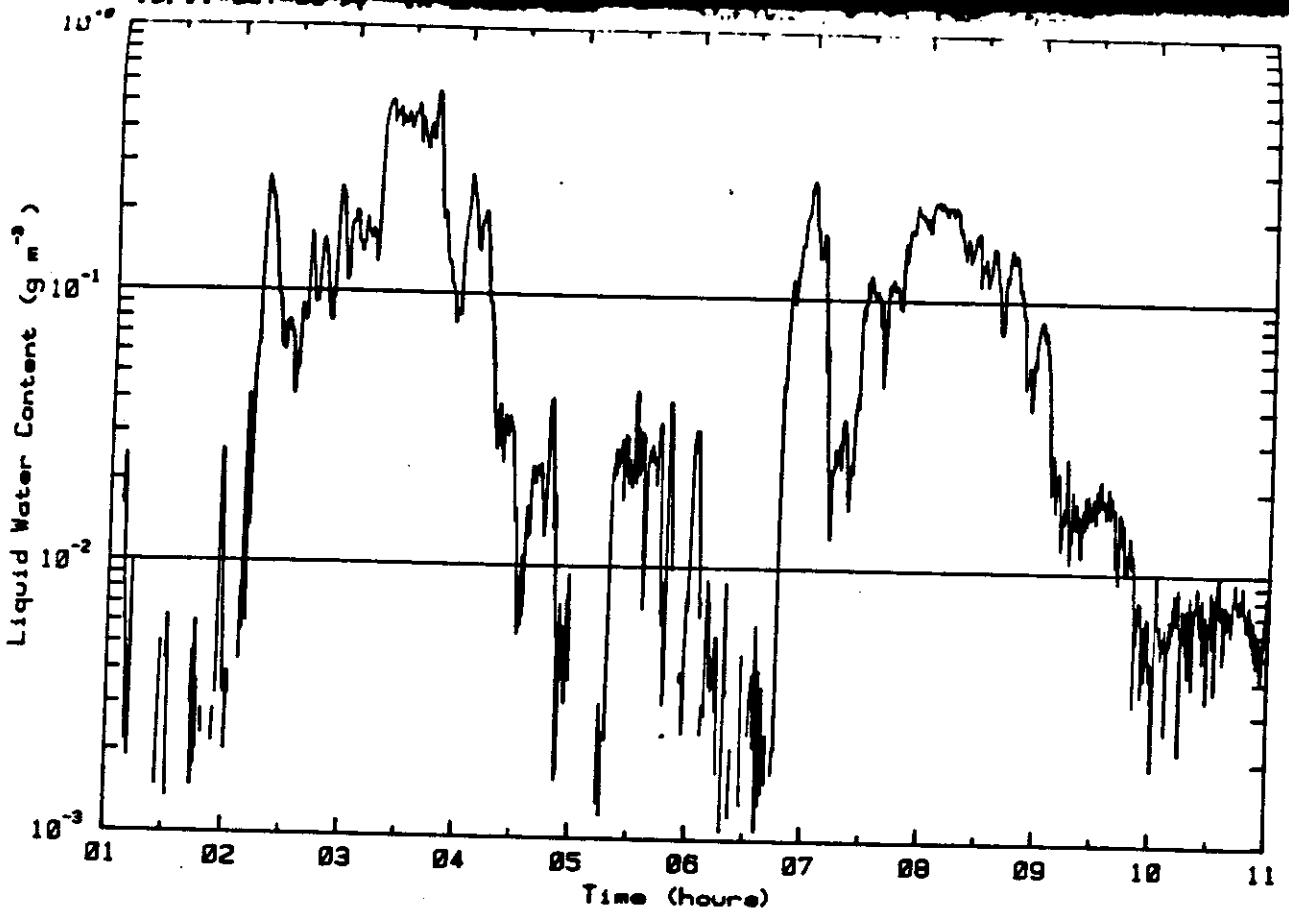

Fig. 5. LWC vs. Time (10-11 Oct 1982)

(5)

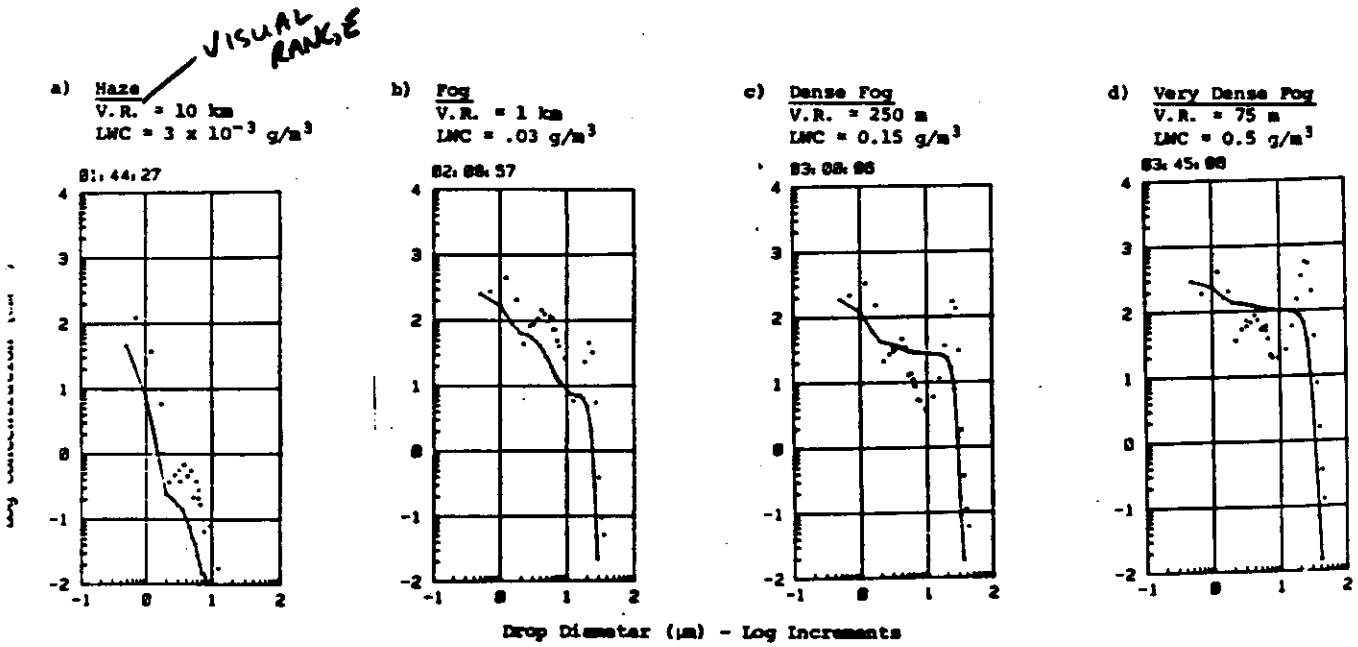

Fig. 7. Drop spectra (FSSP-100) at selected times during evolving dense fog of 10-11 Oct 1983. Solid line curves are cumulative drop concentrations and points are differential dN/d log D concentrations. Independently measured V.R. (AEG) and LWC (I.R. transmissometer) indicated for each time.

ADVECTION FOG – MICROPHYSICS

(FITZGERALD, J. ATM. SCI. 1978, p 1522)

ONE DIMENSIONAL, LAGRANGIAN

NO COALESCENCE, CONST. PARTS.

PRESCRIBED RATE OF INCREASE OF R.H.

① $\frac{ds}{dt} = S' + \left(\frac{ds}{dt}\right)'$

S' ← CONST. INCR.

$\left(\frac{ds}{dt}\right)'$ ← DEPLETION

EXPRESSED IN TERMS OF VAP. MIXING RATIO (x)

→ eq (9)

② $r\frac{dr}{dt}$ for $K_n < 1$ – MODIFIED MAXWELL → eq (10)

③ $\frac{dT}{dt} = -\frac{R^* T^2}{L M_w} S' - \frac{L\left(dx/dt\right)'}{C_{pd} + x C_{pv} + w C_w}$

w – LWC

④ $\left(\frac{dx}{dt}\right)' = -\frac{4}{3}\pi \frac{d}{dt}\int \rho' r^3 n(r)\, dr = -\frac{dw}{dt}$

⑤ Specify CCN spectrum → calc. dry size

→ calc. haze size

CASE STUDIES

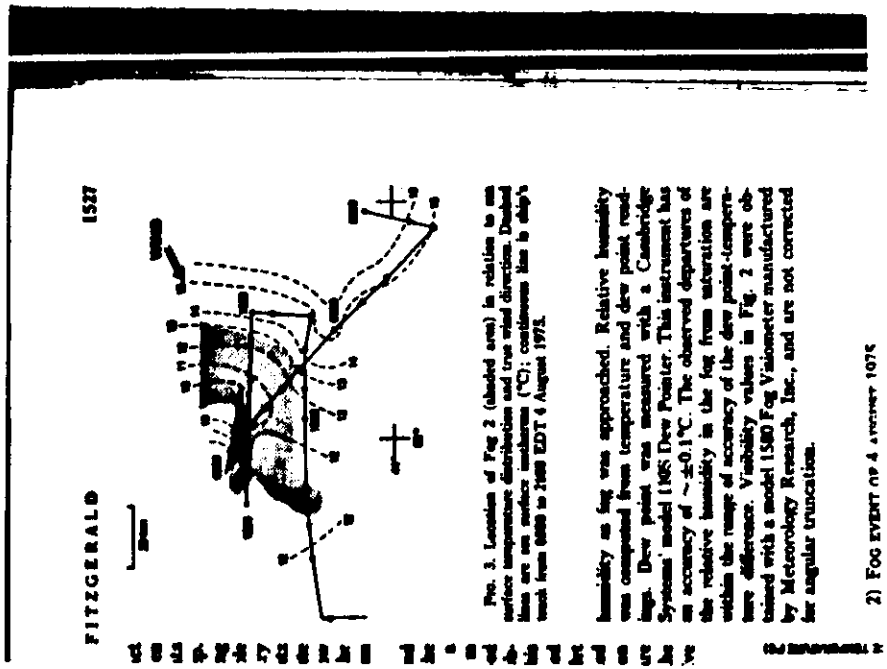

1527 FITZGERALD

Fig. 2. Location of Fog 2 (shaded area) in relation to sea surface temperature distribution and true wind direction. Dashed lines are sea surface isotherms (°C); continuous line is ship's track from 0800 to 2400 EDT 4 August 1975.

humidity as fog was approached. Relative humidity was computed from temperature and dew point readings. Dew point was measured with a Cambridge Systems' model 1106 Dew Pointer. This instrument has an accuracy of ~±0.1°C. The observed departures of the relative humidity in the fog from saturation are within the range of accuracy of the dew point-temperature difference. Visibility values in Fig. 2 were obtained with a model 1530 Fog Visiometer manufactured by Meteorology Research, Inc., and are not corrected for angular truncation.

2) FOG EVENT OF 4 AUGUST 1975

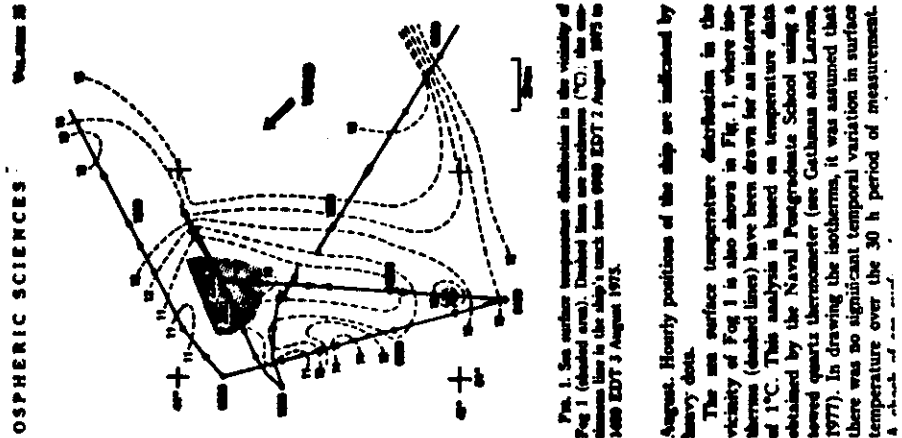

RNAL OF THE ATMOSPHERIC SCIENCES

Fig. 1. Sea surface temperature distribution in the vicinity of Fog 1 (shaded area). Dashed lines are isotherms (°C); the continuous line is the ship's track from 0900 EDT 2 August 1975 to 1400 EDT 3 August 1975.

August. Hourly positions of the ship are indicated by heavy dots.

The sea surface temperature distribution in the vicinity of Fog 1 is also shown in Fig. 1, where isotherms (dashed lines) have been drawn for an interval of 1°C. This analysis is based on temperature data obtained by the Naval Postgraduate School using a towed quartz thermometer (see Cathman and Larson, 1977). In drawing the isotherms, it was assumed that there was no significant temporal variation in surface temperature over the 30 h period of measurement.

(15)

ficient and r the threshold opt the standard value of in (15) assumes the value population, the scattering

$4/3 N Q_0$.

ency factor of a droplet unctional dependence of ffe scattering theory for es of refraction equal to uminated with light of e of Q for droplets larger ues to be 2.00. For the function $Q(r)$ was de- of Q. The value of Q for ues obtained by linearly ecrete values.

ge of the count of Aitken

sively inside and out- e coast of Nova Scotia Navy-sponsored cruise 1975. One of the objec- the data base necessary r the prediction of fogs processing only a small The complete body of of the instrumentation the cruise (Gath-

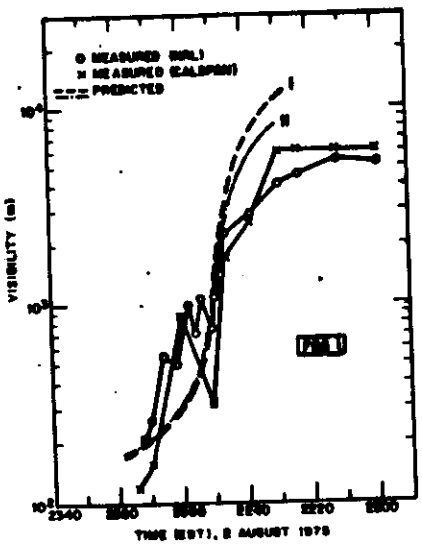

FIG. 7. Comparison of observed and model-predicted visibilities for Fog 1.

test the sensitivity of the computed properties of the fog to a change in the CCN spectrum.

c. Manner in which computed fog properties were related to observations along ship's track

Our computations of the evolution of fog microstructure are initialized at a relative humidity of 98.5%. The predicted properties of the fog at a given point along the ship's path are those exhibited by our model parcel of air after having evolved for a period of time equal to the actual advection time of the air from the 98.5% humidity isopleth to the point of observation. For Fog 1, this isopleth was assumed to pass through the ship's location at 2230 EDT and to run parallel to the 11°C sea surface isotherm along the eastern edge of the fog. In the case of Fog 2, the isopleth of 98.5% relative humidity was assumed to parallel the eastern boundary of the fog at a distance of 8 km upwind (a relative humidity of 98.5% was measured at a distance of 8 km from the fog boundary as fog was approached on the morning of 4 August). Knowing the true wind speed and the distance of the ship from the 98.5% humidity isopleth (as measured along the true wind direction), we can readily compute the advection time.

d. Comparison of observed and model-predicted visibility

Figs. 7 and 8 present comparisons of measured and model-predicted visibilities at a height of ~20 m in Fogs 1 and 2. The NRL measurements were made with the Fog Visiometer, located at the 18.5 m level. This instrument has a factory-stated normal operating range of 70 to 7000 m. Calspan's visibility measurements were made with an EG&G Forward Scatter Meter at a height of 21 m. The range of this instrument is approximately 40 to 6000 m. The Fog Visiometer data in Figs. 7 and 8 have been corrected for angular truncation using correction factors computed by Fitzgerald (1977). This correction is a strong function of droplet size in the range from 2 to 7 μm diameter, but is much less sensitive to droplet size above this range. For a fog composed of droplets >8 μm diameter, the correction factor may be taken to be 1.67 to a suitable degree of accuracy.

It is seen that there is a discrepancy of about a factor of 2 between visibility instruments. While some of this discrepancy is undoubtably due to inherent inaccuracies in the instruments, part of it probably results from differences in the properties of the air reaching the two sensors. As we have already noted, there was a 2.5 m vertical separation between the two instruments. In addition, the Forward Scatter Meter was located slightly forward of the Fog Visiometer and may have had a better exposure to the laminar airflow over the ship.

Figs. 7 and 8 show that the model successfully predicted the evolution of visibility in these two advection fog events. Both the predicted magnitude and time

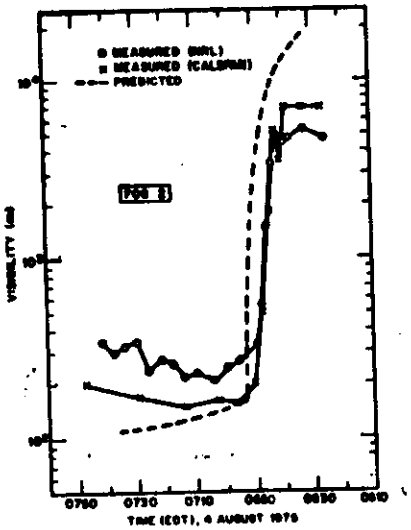

FIG. 8. Comparison of observed and model-predicted visibilities for Fog 2.

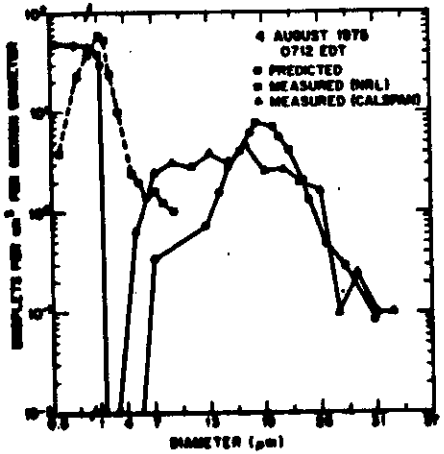

FIG. 10a. Comparison of observed and predicted droplet size distributions in Fog 2 at 0712 EDT 4 August 1975.

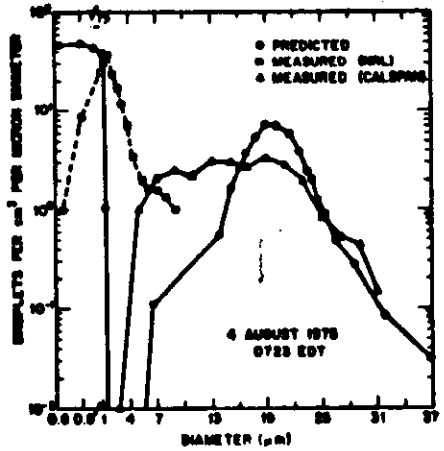

FIG. 10b. As in Fig. 10a except at 0723 EDT 4 August 1975.

which are collected. The lower limit of detection is ~2 μm diameter.

The comparison shown in Fig. 9a is for a location in Fog 1 just several kilometers downwind of the forming edge of the fog. The model-predicted distribution at this point in the fog shows that a separation of activated from unactivated droplets has begun to occur. This is manifested by the appearance of a "shoulder" in the droplet size distribution above 3 μm. Farther downwind, at 2303 EDT (Fig. 9b), this separation has evolved to the point where the droplet distribution has become bimodal. At a distance of 25–30 km downwind of the fog boundary, the predicted spectra show a sharp separation between activated and unactivated droplets, as shown in Figs. 10a and 10b for Fog 2.

The model predicts a large number of unactivated droplets as large as 1.5 μm diameter. That such relatively large droplets are unactivated is explained by the fact that the predicted maximum supersaturation in these fogs is in the range 0.05–0.08%. The largest particle to remain unactivated at a supersaturation of 0.08% has an equilibrium diameter at this supersaturation of ~1.8 μm. In convective clouds, where supersaturations of several tenths of a percent are attained, unactivated droplets will be submicron in size.

Fig. 9b shows that the predicted size distribution of activated droplets in Fog 1 is in excellent agreement with the Calspan impactor data. As can be seen in Figs. 10a and 10b, the agreement between the predicted distributions of activated droplets and the droplet size distributions measured with the impactor is not nearly as good for Fog 2 as for Fog 1. In particular, we note that in Fog 2 the model did not accurately reproduce the breadth of the observed distributions, which exhibited more droplets in the 6–14 μm diameter range than predicted. It should also be noted that the Fog 2 droplet distributions are broader than the Fog 1 droplet distributions. This is probably due in part to

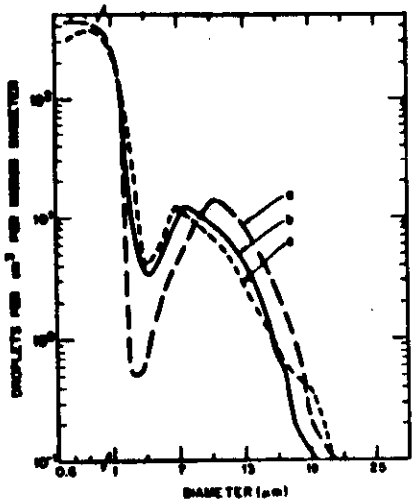

FIG. 11. Comparison of three computed droplet size spectra at 2303 EDT 3 August 1975, showing the effect of a change in input conditions. Curve a: $\beta = 1.37 \times 10^{-3}$ s^{-1}, CCN spectrum I (see Fig. 3); curve b: $\beta = 1.10 \times 10^{-3}$ s^{-1}, CCN spectrum I; curve c: $\beta = 1.10 \times 10^{-3}$ s^{-1}, CCN spectrum II.

RADIATION FOG

(BROWN & ROACH QJRMS 1976 p335
BROWN QJRMS 1980 p781)

ONE-DIMENSIONAL MODEL OF RADIATION & TURBULENT FLUXES,

CONTINUITY EQ'N:

HEAT : RAD^{N} + TURB. EXCH. + LATENT HEAT

VAPOR : TURB. FLUX − CONDENSATE

LIQUID : TURB. FLUX + GRAV. SETTLING^{+} + CONDENSATION

RAD^{N} − EMISSIVITY FROM GROUND 8-13 μm
− ABSORBTION BY AIR 4-8, 13-50 μm
− TRANS. OF H_2O ≈ 1
− " OF DROPLETS

GRAV. SETTLING^{+} : $\overline{V}$ ≈ 6.25 r^2 $|V|$ ≈ cm s^{-1}
$|w|$ ≈ g kg^{-1}

782 R. BROWN

heat, water vapour and liquid water as used in I with additional equations for the
of change of supersaturation, drop radius and concentration.

$$(1)\quad \frac{\partial T}{\partial t} = -\frac{1}{\rho_a c_p}\frac{\partial F_n}{\partial z} + \frac{\partial}{\partial z}\left(K\frac{\partial \theta}{\partial z}\right) + \frac{LC}{c_p}$$

$$(2)\quad \frac{\partial \sigma}{\partial t} = \frac{1}{q_s}\frac{\partial q}{\partial t} - \frac{LM}{R_G T^2}\frac{\partial T}{\partial t}$$

$$(3)\quad \frac{\partial r_{ij}}{\partial t} = \left(\frac{\sigma}{r_{ij}} - \frac{a_1}{r_{ij}^2} + \frac{a_2 m_j}{r_{ij}^3} - a_3 Q_i R\right)(A1 + f_\theta A2)^{-1}$$

$$(4)\quad \frac{\partial N_{ij}}{\partial t} = \gamma r_{ij}^2 \frac{\partial N_{ij}}{\partial z} + \frac{\partial}{\partial z}\left(K\frac{\partial N_{ij}}{\partial z}\right) - \frac{N_{ij}}{\Delta r_i}\left|\frac{\partial r_{ij}}{\partial t}\right| +$$
$$+ \frac{N_{i-1,j}}{\Delta r_{i-1}}\left|\frac{\partial r_{i-1,j}}{\partial t}\right| \quad \text{when } \frac{\partial r_{i-1,j}}{\partial t} > 0$$
or
$$+ \frac{N_{i+1,j}}{\Delta r_{i+1}}\left|\frac{\partial r_{i+1,j}}{\partial t}\right| \quad \text{when } \frac{\partial r_{i+1,j}}{\partial t} < 0$$

$$(5)\quad \frac{\partial w}{\partial t} = \frac{4\pi\rho_l}{3\rho_a}\frac{\partial}{\partial z}\sum_i\sum_j N_{ij} r_{ij}^3$$

$$(6)\quad \frac{\partial G}{\partial z} = \frac{4\pi\rho_l}{3\rho_a}\sum_i\sum_j \frac{\partial N_{ij} r_{ij}^3}{\partial z}$$

$$C = \frac{\partial w}{\partial t} - \frac{\partial G}{\partial z} - \frac{\partial}{\partial z}\left(K\frac{\partial w}{\partial z}\right)$$

$$q = (1+\sigma)q_s$$

$$\frac{\partial q}{\partial t} = \frac{\partial}{\partial z}\left(K\frac{\partial q}{\partial z}\right) - C$$

$$\frac{\partial n_j}{\partial t} = \frac{\partial}{\partial z}\left(K\frac{\partial n_j}{\partial z}\right) - \Delta n_j$$

with T dry bulb temperature of air
θ potential temperature of air
ρ_a density of air
ρ_l density of water
c_p specific heat of air at constant pressure
F_n net radiative flux
z height coordinate with origin at the earth's surface
K exchange coefficient for heat, water vapour and liquid water (assumed equ
L latent heat of vaporization
C rate of condensation per unit mass of air
σ supersaturation
q humidity mixing ratio
q_s saturation humidity mixing ratio
M molecular weight of water vapour
R_G universal gas constant
r_{ij} droplet radius at the centre of the ith bin with nucleus mass m_j
Q_i droplet absorption efficiency factor averaged over wavelength
R net radiation per unit area of drop for unit Q_i
N_{ij} concentration of drops with nucleus mass m_j in the ith bin

γ = v_T/r^2 where v_T is the terminal velocity defined by Stokes Law
Δr_j width of a radius bin
w liquid water mixing ratio
G flux of liquid water due to droplet settling under gravity
n_j concentration of nuclei with mass m_j (i.e. equilibrium radius $<0{\cdot}3\,\mu m$ at ambient relative humidity) Δn_j = concentration of nuclei growing into droplet bins per time step.

The terms on the right-hand side of Eq. (1) represent the change of temperature due to radiative cooling, divergence of the turbulent heat flux and latent heat release. In Eq. (2) the supersaturation changes in response to removal of water vapour and change of temperature. Besides the usual supersaturation, curvature and solute terms Eq. (3) contains an additional term derived by Roach (1976) to allow for the net radiative loss from the droplet. The droplet concentration (Eq. (4)) changes due to the divergences of the gravitational settling flux and the flux due to turbulent diffusion and also by condensational growth or evaporation as prescribed by Eq. (3). The method of solution of Eq. (3) and (4) is described in section (b).

In this paper a cloud condensation nucleus is so designated if it has an equilibrium radius $\leqslant 0{\cdot}3\,\mu m$ at the ambient supersaturation. According to Eq. (10) nuclei are diffused but their gravitational settling is ignored. They play no part in the model thermodynamics or radiative processes but merely act as a source of droplets. The growth of the nuclei is not calculated explicitly, they are adjusted to their equilibrium radius at the ambient supersaturation at each radiation time-step. Those with an equilibrium radius $\geqslant 0{\cdot}3\,\mu m$ are reclassified as drops and placed in the appropriate radius bin. Here they grow by condensation, release latent heat, settle under gravity and are subject to turbulent diffusion.

The coefficients in Eq. (3) are:

$$a_1 = \frac{2SM}{\rho_l R_G T}$$

$$a_2 = 6{\cdot}05\times10^{-5}\ \mathrm{m^3\,kg^{-1}}$$

$$a_3 = \frac{1}{kT}\left(\frac{LM}{R_G T}-1\right)$$

$$R = \tfrac{1}{2}(F\uparrow + F\downarrow) - sT^4$$

$$Qi = 1{\cdot}18\{1-\exp(-0{\cdot}28r)\}$$

$$A1 = \frac{L\rho_l}{kT}\left(\frac{LM}{R_G T}-1\right)$$

$$A2 = \frac{\rho_l R_G T}{DMe_s(T)}$$

$$f_\beta = 1 + l_\beta/r_{1j}$$

$$l_\beta = \left(\frac{2\pi M}{R_G T}\right)^{\frac{1}{2}}\frac{D}{\beta}$$

with
S surface tension of pure water
k thermal conductivity of air
$F\uparrow, F\downarrow$ upward and downward longwave fluxes at height Z
s Stefan–Boltzmann constant
D diffusivity of water vapour in air
$e_s(T)$ saturation vapour pressure at temperature T
β condensation coefficient

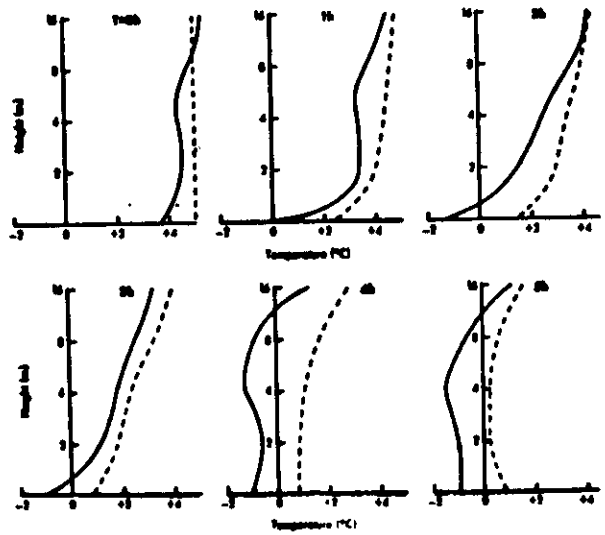

Figure 3. Comparison of the development of the observed and model predicted temperature profiles: ——— observed temperature profile; - - - - model predicted temperature profile. The time in hours above the profiles refers to the interval from the start of the integration or from the time of cloud clearance (0830 GMT) on 7 December 1971.

non-radiative heating rates are compared in Fig. 4. As may be expected the behaviour of the computed heating rates is more regular than those observed but both exhibit a tendency for the observed cooling rate to be less than the radiative cooling rate. There is some discrepancy in the behaviour of the heating rates during the first ninety minutes which may be due to the earlier development of fog on 7 December. The evidence of this comparison indicates a tendency for the model to underestimate the magnitude of the radiative cooling. The comparison has been terminated at 0830 GMT because beyond this time the influence

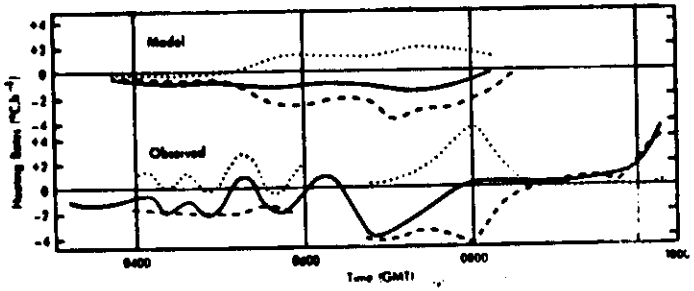

Figure 4. Comparison of the observed heating rates on 7 December 1971 averaged over the 2·9m layer with the model predicted heating rate at 4m: ——— total heating rate; - - - - radiative heating rate; ..... non-radiative heating rate.

of solar insolation will become more noticeable in the observed heating rates. Up to this time the effect of solar insolation should be small and it is believed that the reduction in radiational cooling rate after 18 h is primarily due to the increased optical depth of the fog.

There is a noticeable disagreement between the behaviour of the fog top computed by the model and that observed in nature. The latter is often observed to be quite sharply defined, but because of decreasing vertical resolution with height the model cannot produce well defined fog tops. Furthermore it is probable that the nature of the fog top is partly controlled by the decrease in turbulent mixing associated with the inversion below the fog top.

Because of the more realistic results obtained with model III this model is used in all further integrations described in this paper unless otherwise stated.

(b) *The role of radiative cooling*

Assuming that the ground but not the air can cool by radiation, the model was integrated for twelve hours. No fog had formed at the end of this period although the lowest layers of the atmosphere were close to saturation. Since on the 7 December 1971 fog was

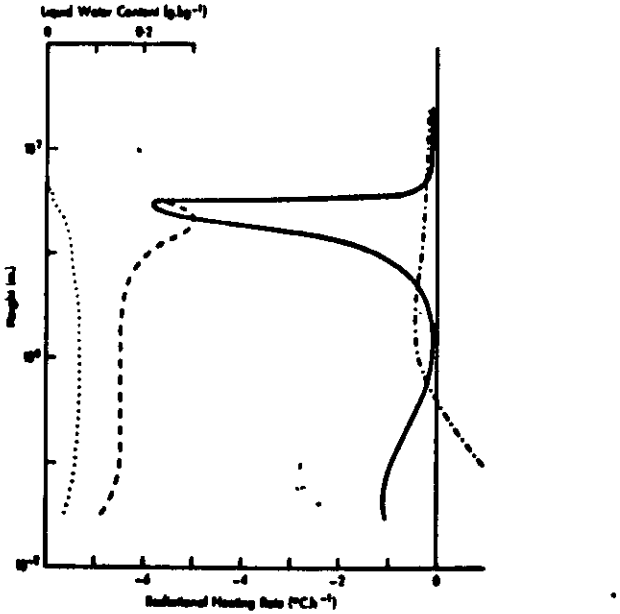

Figure 5. Illustration of the effect of the omission of liquid water radiation upon the model predicted liquid water content and radiational heating rate after five hours integration.
——— radiative heating rate
– – – – liquid water content
} liquid water radiation included
–·–·–· radiative heating rate
····· liquid water content
} liquid water radiation omitted.

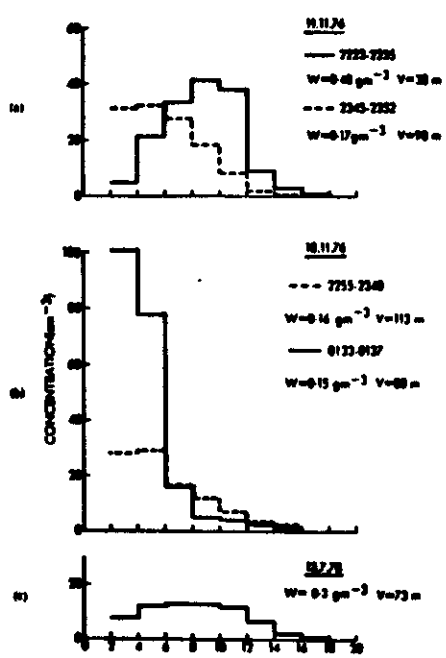

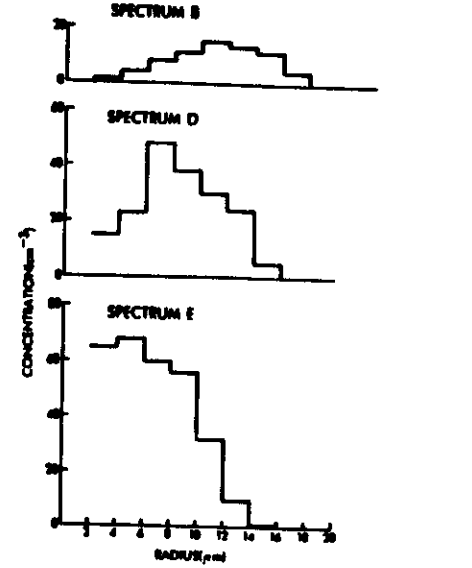

Figure 7. Examples of drop-size distributions obtained during the Cardington Fog Project. Each distribution is a mean over the period shown of data obtained at 10 s intervals.

Drop-size distributions at a height of 2 m after four hours integration. Each distribution is for a different nucleus concentration as annotated

tration of nuclei. This does not imply that the reduction in visibility is brought about wholly by the redistribution of available water as a high concentration of small drops. Although this is partly the reason, there is also an increase in liquid water content. For example with spectrum E the maximum liquid water content is increased by 20%, and the average over the course of the integration by 50%.

As anticipated, increasing the nucleus concentration produces a drop-size distribution with a higher drop concentration and smaller mean radius. The spectra at 2 m after four hours integration in Fig. 6 illustrate this. At this time the fog is 100 m deep. Some of the previous investigations considered the growth of drops in an ascending parcel of adiabatic cooling produced the supersaturation necessary for droplet growth. nucleus concentration affected the growth of the droplets by increasing the the available water. In this numerical study radiative cooling is the driving growth. Thus it is possible that variations in nucleus concentration may growth by altering the radiation field

Integrations has been performed using a nucleus spectrum of constant al concentration. The spectra used were (B), (D) and (E) the latter two two-and-a-half and five times (B) respectively. As the nucleus concen- peak supersaturation is lowered, for example from 0·05% to 0·03% visibility is reduced. Fig. 5. For a fixed liquid water content it is ility is proportional to N^{-1} where N is the droplet concentration. minimum visibility is proportional to N_c^{-1} where N_c is the concen- tra